An Ionosphere Specification Technique Based on Data Ingestion Algorithm and Empirical Orthogonal Function Analysis Method.

Ercha Aa,[1,2] Aaron Ridley,[2] Wengeng Huang,[1] Shasha Zou,[2] Siqing Liu,[1,3]

Anthea J. Coster,[4] and Shunrong Zhang[4]

Correspondence to: E. Aa (aercha@nssc.ac.cn)

[1]National Space Science Center, Chinese Academy of Sciences, Beijing, China.

[2]Department of Climate and Space Sciences and Engineering, University of Michigan, Ann Arbor, MI, USA.

[3]College of Earth and Planetary Science, University of Chinese Academy of Sciences, Beijing, China.

[4]Haystack Observatory, Massachusetts Institute of Technology, Route 40 Westford, MA, USA.

Abstract. A data ingestion method in reproducing ionospheric electron density and total electron content (TEC) was developed to incorporate TEC products from the Madrigal Database into the NeQuick 2 model. The method is based on retrieving an appropriate global distribution of effective ionization parameter (Az) to drive the NeQuick 2 model, which can be implemented through minimizing the difference between the measured and modeled TEC at each grid in the local time – modified dip latitude coordinates. The performance of this Madrigal TEC-driven-NeQuick 2 result is validated through the comparison with various International GNSS Services (IGS) global ionospheric maps (GIMs) and ionosonde data. The validation results show that a general accuracy improvement of 30-50% can be achieved after data ingestion. In addition, the empirical orthogonal function (EOF) analysis technique is used to construct a parameterized time-varying global Az model. The quick convergence of EOF decomposition makes it possible to use the first 6 EOF series to represent over 90% of the total variances. The intrinsic diurnal variation and spatial distribution in the original data set can be well reflected by the constructed EOF base functions. The associated EOF coefficients can be expressed as a set of linear functions of $F_{10.7}$ and Ap indices, combined with a series of trigonometric functions with annual/seasonal variation components. The NeQuick TEC driven by EOF modeled Az shows 10-15% improvement in accuracy over the standard ionosphere correction algorithm in the Galileo navigation system. These preliminary results demonstrate the

effectiveness of the combined data ingestion and EOF modeling technique in improving the specifications of ionospheric density variations.

1. Introduction

The Earth's ionosphere is a highly variable region of space that exhibits both climatological variations and weather disturbances. In order to better mitigate the detrimental effects of the ionosphere on radio propagation and satellite navigation, it is of great importance to provide timely and reliable ionospheric specification and prediction through utilizing various ionospheric empirical and/or theoretical models. Ionospheric empirical models, such as International Reference Ionosphere (IRI) [*Bilitza*, 2001; *Bilitza and Reinisch*, 2008] and NeQuick [*Di Giovanni and Radicella*, 1990; *Radicella and Leitinger*, 2001; *Nava et al.*, 2008], are mainly built on the basis of statistical analysis of large data sets. Empirical models have the merits of simplicity and accuracy in reproducing the climatological characteristics of the ionosphere, yet are limited to the way the suitable function was chosen and the quality of the data that were used. Ionospheric theoretical models are constructed on the basis of fundamental physical laws (mass balance, energy balance, heat transfer relations, etc.), and can be run under a much wider set of conditions to test the theories, yet are limited by a lack of accurate estimation of the external drivers and initial conditions. With the continuous increase of ionospheric measurements from diverse sources, such as the total electron content (TEC) data from ground-based Global Navigation Satellite Systems (GNSS) networks, radio occultation data from low-Earth orbit (LEO) satellites, global digisonde profiles, in situ Ne measurements, and ultraviolet (UV) airglow data, it has been realized that the dynamic processes and subtle variations in the ionosphere could be better specified and predicted through data assimilation/ingestion techniques to incorporate ionospheric observations into background models [e.g. *Nava et al.*, 2011; *Yue et al.*, 2012; *Schunk et al.*, 2014].

Data assimilation and ingestion techniques are usually associated with each other yet not clearly distinguished. For data assimilation, the observations are projected by certain optimization algorithm (e.g. Kalman filter, 3D/4D variational method) into proper global or regional scales to get a best estimation of the external drivers and initial/boundary conditions of the first-principle ionospheric models. For example, Utah State University (USU) constructed a Global Assimilation of Ionospheric Measurements (GAIM), which uses a physics-based Ionosphere Forecast Model (IFM) and a Kalman filter as a basis for assimilating a diverse set of near real-time measurements [*Scherliess et al.*, 2004; *Schunk et al.*, 2004, 2005; *Scherliess et al.*, 2006]. The Jet Propulsion Laboratory and University of Southern California have cooperatively constructed another Global Assimilation Ionospheric Model (JPL/USC GAIM), which uses a traditional Kalman filter method to estimate the three-dimensional density state, and a four-dimensional variational approach (4DVAR) to estimate ionospheric drivers such as neutral winds and the equatorial E$\times$B drift [*Pi et al.*, 2003; *Wang et al.*, 2004; *Mandrake et al.*, 2005]. Some studies use sophisticated empirical models to define the a priori state in order to implement data assimilation, such as Ionospheric Data Assimilation Three-Dimensional (IDA3D) [*Bust et al.*, 2004, 2007], Electron Density Assimilative Model (EDAM) [*Angling and Cannon*, 2004; *Angling and Khattatov*, 2006], North American/United States TEC (NATEC/USTEC) [*Fuller-Rowell et al.*, 2006], and China assimilation TEC Model (CNTEC) [*Aa et al.*, 2015, 2016]. Moreover, there are extensive studies that described the development of ionospheric and thermospheric data assimilation models/procedures [e.g., *Pi et al.*, 2009;

Komjathy et al., 2010; *Yue et al.*, 2011, 2012; *Lee et al.*, 2012; *Matsuo et al.*, 2012; *Zhu et al.*, 2012; *Schunk et al.*, 2014].

However, developing an ionospheric data assimilation model is very complicated with many trade-offs and approximations. The computational ease and simplicity makes data ingestion techniques readily accessible to the wide audience of space weather research and application communities. Generally, data ingestion differs from data assimilation in the following two aspects: first, instead of using complex physics-based models, data ingestion usually uses simplified and parameterized models in terms of a given set of "effective" driven factors; second, data ingestion usually drives the background model towards experimental data sets by using a simple optimization algorithm such as least-square estimation to minimize the deviations between experimental and model values, which has the merits of computation efficiency in contrast to time-consuming calculation in an assimilation process that involves complicated error covariance matrices. There are some studies that ingested global ionosonde measurements into the IRI empirical model. For example, the IRI real-time assimilative mapping (IRTAM) incorporate data from the Global Ionospheric Radio Observatory (GIRO) to adjust the Consultative Committee of International Radio (CCIR) coefficients [*Galkin et al.*, 2012]. Moreover, some studies adapted the NeQuick empirical model by ingesting GNSS-derived slant TEC [*Nava et al.*, 2006], global ionospheric maps (GIMs) of vertical TEC [*Nava et al.*, 2005], and COSMIC-derived radio occultation TEC/Ne [*Brunini et al.*, 2011; *Nava et al.*, 2011]. Although these NeQuick data ingestion attempts are able to improve the model capability in specifying three-dimensional ionospheric Ne by updating the ionization level parameters Az, there are a few things that worth noting: 1) Since preliminary fitting and approximations are needed to generate vertical TEC GIMs, ingesting these "secondary" data could get complete global *Ne* profiles, but with compromises in accuracy and resolution; 2) Ingesting GNSS-derived slant TEC can improve the accuracy of the reconstructed global ionospheric *Ne* with acceptable computation, though it is more suitable at a single station or over regional grids. Therefore, in the current study, we will use a modified data ingestion technique to adapt the NeQuick 2 model by ingesting TEC products derived from the Madrigal Database of the Massachusetts Institute of Technology (MIT) Haystack Observatory, then an Empirical Orthogonal Function (EOF) analysis method will be used to give time-dependent specifications of the three-dimensional electron density of the ionosphere. We aim to make this product applicable to precisely reproducing the global ionospheric morphology for scientific study and to providing an alternative ionospheric correction algorithm for GNSS single-frequency users.

The rest of the paper is organized as follows: the NeQuick 2 model and Madrigal TEC data will be briefly introduced in section 2. The data ingestion technique and its validation will be given in section 3. The EOF modeling method and its verification will be presented in section 4 and the conclusions in section 5.

2. Description of the model and data

The NeQuick 2 [*Nava et al.*, 2008] is used here as a background model to describe the global distribution of electron density. The NeQuick 2 model is developed at the Aeronomy and Radio propagation Laboratory of the Abdus Salam International Centre for Theoretical Physics (ICTP), Trieste, Italy, and at the Institute for Geophysics, Astrophysics and Meteorology (IGAM) of the University of Graz, Austria. NeQuick 2 describes the vertical profile of bottomside *Ne* in terms of a modified DGR profile formulation [*Di Giovanni and*

Radicella, 1990; *Radicella and Leitinger*, 2001], which includes five semi-Epstein functions with modeled thick parameters to represent the lower and upper parts of the E and F1 layers, as well as the lower part of the F2 layer. The functions are anchored to the N_m (electron density) and the h_m (height) of the E, F1, and F2 layer peaks, which can be either experimentally derived from ionosonde measurement, or modeled as indicated by *Leitinger et al.* [2005]. The topside ionosphere is represented by a sixth semi-Epstein function with a height-dependent thickness parameter that can be empirically determined as described by *Coïsson et al.* [2006]. The basic inputs of the NeQuick 2 model are: position, time and solar flux (or sunspot number); the outputs are the electron density along the ray-path and the numerically integrated TEC. For more details about NeQuick 2, readers may refer to *Nava et al.* [2008] and the references therein.

The TEC products derived from the Madrigal database are used here for data ingestion, which are developed at the Massachusetts Institute of Technology (MIT) Haystack Observatory by using dense networks of worldwide GNSS receivers [*Rideout and Coster*, 2006; *Vierinen et al.*, 2016]. The gridded TEC cover locations where GNSS data are available and have a resolution of 1°(latitude) × 1°(longitude)× 5 min. Madrigal gridded TEC is strictly data driven with no postprocess interpolation or fitting that might smooth out real gradients, which can thus be considered as a suitable TEC source for data ingestion.

3. TEC ingestion technique and validation

For a given time and location, the TEC value derived from the integration of NeQuick 2 electron density profile varies monotonically as a function of the 10.7 cm solar radio flux. For the technique presented here, the optimum solar flux that produces the best TEC value from NeQuick 2 is usually termed as Az, which is an effective parameter to represent local ionization level and is calculated by minimizing the Root Mean Square Error (RMSE) between the modeled and observational TEC [*Nava et al.*, 2005, 2006]:

$$RMSE = \sqrt{\frac{1}{N}\sum_{i=1}^{N}(TEC_{mod}(Az) - TEC_{obs})^2}, \quad (1)$$

Here N is the number of individual observations during the current interval. Figure 1a illustrates the process in calculating the minimum RMSE to derive Az. As an example to quantitatively illustrate the effect of data ingestion, Figure 1c shows the RMSE comparison between NeQuick 2 driven by $F_{10.7}$ (red) and driven by Az (black) at a GNSS station: BJFS (39.4°N, 115.9°E) during September 02-10, 2017. It can be seen that the RMSE calculated via using a modified Az to drive NeQuick 2 is generally 30-50% smaller that the model driven by the observed $F_{10.7}$. This partly demonstrates the systematic improvements when TEC data are ingested into the NeQuick 2 model.

In the traditional TEC ingestion method, the above-mentioned technique is either applied to all grids of vertical TEC GIMs (normally 2.5° in latitude and 5° in longitude) to get a global distribution of Az maps [e.g. *Nava et al.*, 2005; *Yu et al.*, 2015], or applied to slant TEC at a single or multiple GNSS stations to get a scattered Az distribution that might be further interpolated or fitted into regular size [e.g. *Nava et al.*, 2006; *Nigussie et al.*, 2016]. Both of these techniques focus on obtaining fixed geographical distribution of Az to drive NeQuick to get 3D specification of the ionospheric electron density. However, the extent of photoionization and ionospheric dynamics are also strongly dependent on the geomagnetic field and local time. *Rawer* [1963] proposed a parameter called the modified dip latitude μ (Modip), which combines the geomagnetic dip I and the geographic latitude ϕ

$$Modip = arctan(\frac{I}{\sqrt{cos\phi}}). \tag{2}$$

Thus, in order to consider both the geomagnetic field and the spinning of Earth, the current study will use local time-Modip coordinate system to represent the variation of Az instead of using simple geographic or geomagnetic coordinates. The grid points are spaced 5° in Modip latitude by 0.5 h in local time. For a certain day, the Madrigal TEC within each grid will be used to derive the Az on the basis of the above-mentioned data ingestion technique, then global LT-Modip maps of Az and associated RMSE distribution can be generated accordingly. Figure 2a illustrates an example of the Az distribution on September 02, 2017 ($F_{10.7}$ = 120). Figures 2b and 2c show the associated RMSE after and before TEC ingestion, respectively. It can be seen from Figure 2a that Az has relatively large values around the auroral zone and equatorial ionization anomaly (EIA) regions. This might be due to the fact that NeQuick 2 is only using solar radio flux as the effective driver, as well as that the NeQuick 2 model does not include the effect of ionization enhancement around 125 km due to particle precipitation. So in this case, the model may be expected to underestimate the electron density around the auroral and EIA regions, which need to be compensated via the enhancement of Az.

Furthermore, the following characteristics on modip latitude distribution can also be seen from the figure. First, for the equatorial and low latitude regions (∼30°S-30°N), the Az values are generally lower than $F_{10.7}$. Similar to the EIA, there are double-peak structures near the EIA crest both for RMSE_{Az} (∼10 TECU) and $\text{RMSE}_{F10.7}$ (∼20 TECU), while the RMSE values around the equator are much lower. Second, for mid-to-high latitude bands, there is a hemispheric asymmetry in the Az distribution especially around the auroral zones, with the northern hemisphere exhibiting relatively larger Az values (close to real $F_{10.7}$) than those of the southern hemisphere. This might be ascribed to relatively higher numbers of GNSS observations in the northern hemisphere both in the Madrigal database and used to construct the NeQuick 2 model. It could also be that the performance difference of the model was due to the effect of seasonal and hemispheric variation of precipitation in the auroral zone. Moreover, the RMSE have relatively lower values for mid-to-high latitude bands, while the polar regions have lower Az and RMSE values.

Figure 2d shows a scatter plot of the comparison between RMSE_{Az} and $\text{RMSE}_{F10.7}$, while the color represents the percentages ratio of RMSE_{Az} to $\text{RMSE}_{F10.7}$. Through adjusting Az values, the data ingestion method generally reduced the errors around 50% since most of the points have green-to-blue colors. Another important thing worth noting is that the local time variation of Az is usually ignored in the past ingestion method, where Az at a fixed location will be updated by using 24 hours of data and then expressed as a sole function of Modip latitude. Thus the diurnal variation of errors was smoothed out to a great extent in this way. However, it can be seen from Figure 2a that the optimized Az has an obvious local time variation pattern. For equatorial and low latitude regions, Az has relatively large values around the local noon sectors, which could be attributed to the EIA enhancement. For mid-to-high latitude regions, Az has maximum values around local night hours, which might indicate that NeQuick 2 tends to underestimate (overestimate) ionosphere electron density during nighttime (daytime) around these latitudinal regions, since NeQuick 2 did not include the effects of ionization enhancement around 125 km due to particle precipitation.

With the availability of the optimized Az distribution map, the local ionization level for different locations and times can be derived correspondingly, and the Madrigal-driven NeQuick 2 results can then be generated by using derived Az as model inputs. Figure 3 gives an example of the reproduced global 3D electron density in latitude/height slices, F2 layer critical frequency (foF2), and the vertical TEC map at 0230 UT on 02 September 2017. It can be seen that the large-scale features of ionosphere such as the EIA and hemispheric asymmetry could be reasonably reproduced. Since TEC measurements were used for data ingestion, it is expected that comparisons with TEC would be better than comparisons with electron density profiles.

3.1. Comparison with IGS GIMs

In order to verify the validity of the data ingestion technique, the TEC GIMs provided by International GNSS Services (IGS) are used here to make a comparison. Currently, there are five IGS ionospheric analysis centers routinely providing TEC GIMs by using ever-growing measurements from dense GNSS receivers. These centers include the Center for Orbit Determination in Europe (CODE), European Space Agency (ESA), Jet Propulsion Laboratory (JPL), Polytechnical University of Catalonia (UPC), and Chinese Academy of Sciences/Wuhan University (CAS/WHU). The TEC GIMs of CODE and ESA are modeled by using a series of Spherical Harmonic (SH) functions up to degree and order of 15 [*Feltens and Schaer*, 1998; *Schaer*, 1999; *Feltens*, 2007]. JPL adopted a grid-based modeling method to represent the TEC by using a linear composition of bi-cubic splines with 1280 spherical triangles [*Mannucci et al.*, 1998; *Komjathy et al.*, 2005]. The approaches used by UPC are similar to those of JPL, while UPC modeled the ionospheric TEC variation over each station separately by using a rectangular grid of two layers [*Hernández-Pajares et al.*, 1999, 2009]. CAS GIMs are generated by using a function-based plus grid-based approach that combine the Spherical Harmonic functions and the generalized Trigonometric Series functions [*Li et al.*, 2015].

As a preliminary verification of the data ingestion method, around 10% of the Madrigal TEC data set was selected as a control group (i.e., not used for data ingestion). Then the IGS GIMs and data ingestion TEC results were compared with the control group, respectively. Figure 4 shows the histogram statistics of the comparison on 02 September 2017. The data ingestion errors ($\mathrm{TEC}_{NEQ(Az)}$-$\mathrm{TEC}_{Madrigal}$) exhibit a nearly unbiased Gaussian distribution with relatively low mean value (0.22 TECU) and standard deviation (2.14 TECU). The different IGS errors are generally more skewed and dispersed with larger standard deviation values.

In order to get a more comprehensive comparison under different solar and geomagnetic activities, Figure 5 displays the RMSE results of IGS GIMs and data ingestion TEC with respect to the Madrigal control group during the time interval from August 25 to September 10, 2017. The temporal variation of $F_{10.7}$ and 3-hour ap index for this interval are showen in Figure 5a. The $F_{10.7}$ gradually increased from $\sim$80 to 140, then decreased to 107. Meanwhile, the ap index has two peaks of 207 and 236, which correspond to a double main phase of an intense geomagnetic storm on 07-08 September 2017. Thus this time interval covers varied levels both for solar and geomagnetic activities, which is a suitable period to test the effectiveness of the data ingestion technique. Figure 5b shows that the RMSE of the data ingestion technique is generally smaller (around 1 TECU) than those of IGS GIMs, while all products have relatively large errors during the storm time. One thing worth noting is that the differences between data ingestion results and IGS GIMs could be caused by systematic errors that are generated by different processing algorithms of biases correction. The GIMs of JPL and UPC have larger mean bias: ∼3 TECU and ∼2.5 TECU, respectively, while those of ESA (∼2.2 TECU), CODE (∼1.8 TECU) and CAS (∼1.5 TECU) are relatively smaller. For more details about the bias of different IGS GIMs, readers may refer to *Li et al.* [2015] and *Hernández-Pajares et al.* [2009]. Also, the control group might not be strictly "independent" due to possible interference from surrounding measurements. Therefore, this initial comparison might indicate the effectiveness of data ingestion technique, though further comparisons are still needed.

3.2. Comparison with Ionosonde data

Ionospheric foF2 measured by ground-based ionosonde can be considered as a suitable reference to verify the data-ingestion results. Six ionosonde stations at different latitude/longitude locations were used to make the comparison. Figure 6 shows the comparisons of ionosonde foF2 measurements with those calculated via NeQuick 2 driven by $F_{10.7}$ (red) and Az (blue) during August 25 to September 10, 2017. The RMSE, correlation coefficient, as well as the geographic coordinates are marked in the figure. Generally, the data ingestion results had relatively lower RMSE values and higher correlation coefficients, which illustrate that the ability of NeQuick 2 in reconstructing the foF2 is also improved after the Madrigal TEC are ingested into the model.

4. EOF modeling of Az

The data ingestion is basically a now-casting method of measurement update. Considering the forecasting needs of ionospheric correction for navigation and communication customers, it is of great importance to construct a time-dependent model of Az so that the spatiotemporal variability after previous TEC ingestion could be extracted and parameterized to make a prediction for future use. In this study, the Empirical Orthogonal Function (EOF) analysis technique, also known as Principal Component Analysis (PCA) method, was used to build this time-dependent Az model. The EOF technique is a statistical procedure, capturing the most significant components of the variability in the original data set, which is implemented by using an orthogonal transformation to decompose the original data set into a series of uncorrelated base functions, with each succeeding base function accounting for as much residual variance as possible [*Jolliffe*, 1990]. The merit of the EOF technique is that it converges quickly, which makes it possible to succinctly represent the majority of the original variances by using only a few base functions and associated coefficients. For more details about the mathematical explanation of the EOF analysis method, readers may refer to *Dvinskikh* [1988] and *Singer and Dvinskikh* [1991] and the references therein.

In order to get a balance between capturing the variances as much as possible and making ionospheric "weather" prediction, the Az data set needed an appropriate time length. Using multiple years of Az data to do EOF decomposition would generate the maximum variances, yet making this model a "climatological" one. On the other hand, if the time length of Az data was too short, then it would be unlikely to extract effective base functions with enough variances to make the forecast. Thus in the current study, after above-mentioned Madrigal TEC ingestion, a moving data set of Az ratio (i.e. $Az/F_{10.7}$) with a time length of 81-days was reorganized into the following matrix Az_{ratio}(LT, modip, d), in which LT, modip, and d stand for the local time (48 grids), modified dip latitude (36 grids), and day of year (81 days), respectively. This Az_{ratio} data set could then be decomposed into EOF base functions and associated coefficients:

$$Az_{ratio}(LT, modip, d) = \sum_{i=1}^{N} EOF_i(LT, modip) \times Coef_i(d), \tag{3}$$

where EOF_i(LT,modip) is the i_{th} EOF base functions that vary with local time and modified dip latitude, which represent the diurnal fluctuation and spatial distribution of original data set. $Coef_i(d)$ is the associated i_{th} coefficient that indicates the temporal variation of original data set. N is the total number of EOF decomposition series. The order of the EOF series is ranked according to their variance, and the variances contributed by the first 6 EOF series are listed in Table 1. Since 91.77% of the total variance in the original data set can be reproduced via the first 6 EOF series, so it is an effective and efficient modeling method to use only six EOF base functions and coefficients to represent most of the variation in the original data set.

Figure 7 shows the modip latitude and local time distribution of the first 6 EOF base functions. Take EOF 1 to EOF 3 as example, EOF 1 appears to represent the most dominant feature of global spatial and temporal variation of the original data set, which is day-to-night variability as well as high-latitude-to-low-latitude difference due to solar ionization. EOF2 mainly displays hemispheric asymmetries, which can be attributed to the summer-to-winter annual variation induced by the uneven solar EUV illumination. EOF 3 captures mostly auroral and high latitude variations, which can be ascribed to Joule heating and auroral precipitation under the influence of geomagnetic activity. EOF 4 – EOF 6 have similar distribution features but with more small-scale variations. The physical meaning of these EOF components are not always apparent, particularly for high order ones whose contributions to the overall variance in the data are often very small. Figure 8 shows the temporal variation of the first 6 EOF coefficients. The corresponding

$F_{10.7}$ is also plotted in Figure 8a for comparison. The $Coef_1$ and $F_{10.7}$ are roughly anti-correlated, which indicate that there are certain variations in the original data set that are dependent on solar activity. In order to further investigate the intrinsic dependence of Az_{ratio} on solar and geomagnetic activity, Table 2 gives the correlation values of the first 6 EOF coefficients with respect to $F_{10.7}$ and daily Ap index. The correlation between $Coef_1$ and the $F_{10.7}$ index is -0.96, while all coefficients more or less have some correlation with Ap index. This shows that the local ionization parameter Az changes mainly as a function of solar activity, while geomagnetic activity also plays a non-negligible role in affecting it.

Therefore, the first 6 EOF coefficients could be parameterized and modeled as follows:

$$Coef_i(d) = F^i_{SG} \times F^i_{time}, \tag{4}$$

where F^i_{SG} represents the effects of solar and geomagnetic activity, and F^i_{time} refers to annual/seasonal variations. These two parameters can be expressed as follows:

$$F^i_{SG} = a_i + b_i F_{10.7}(d) + c_i Ap(d), \tag{5}$$

$$F^i_{time} = d_i + e_i cos(\frac{2\pi d}{365.25}) + f_i sin(\frac{2\pi d}{365.25}) + g_i cos(\frac{2\pi d}{81}) + h_i sin(\frac{2\pi d}{81}), \tag{6}$$

where *a*-*h* are amplitudes of various terms in the above equations and can be calculated via a multiple linear regression analysis method. Thus the EOF coefficients can be expressed as a parameterized function of $F_{10.7}$ and Ap index, which can be reconstructed with observed or predicted $F_{10.7}$ and Ap index. Figure 8 also shows an example of reconstructed EOF coefficients as dashed lines, which agrees well with the original solid lines. In this way, for the time-window of 81 days, the naturally decomposed EOF base functions and artificially fitted coefficients can be combined with each other to generate modeled Az values, which can then be used to drive the NeQuick 2 model to make a short term prediction of Ne and TEC for the next day (or even longer). This whole procedure of data ingestion and EOF modeling can be rolled over with a moving time-window.

In order to verify the effectiveness of the EOF modeling technique, the Az modeling method of the Galileo navigation system is introduced here to make a comparison. In the Galileo ionospheric correction algorithm, the Az values of the previous day are expressed as a 2_{nd} order polynomial function of Modip: $Az = a_0 + a_1 \times modip + a_2 \times modip^2$, then the set of 3 coefficients are calculated and broadcasted in the navigation file so that the ionospheric delay at a specific frequency for the next day can be corrected using NeQuick driven by reconstructed Az parameters [*Bidaine and Warnant*, 2011]. Figure 9 shows the temporal variation of RMSE comparison between NeQuick TEC driven by EOF modeled Az (solid line) and that driven by polynomial fitted Az (dashed line) during the time period of August 25 – September 10, 2017. The NeQuick RMSE driven by the EOF modeled Az are generally smaller than those of the polynomial fitted Az with an average improvement of ∼10–15%. Both of which have larger errors around the geomagnetic storm time, which is consistent with those indicated in Figure 5. Moreover, considering the polynomial method needs fewer parameters transmitted to the users, it is still more functional in real application.

5. Conclusion

In this paper, a data ingestion technique is described to incorporate the Madrigal TEC data into the NeQuick 2 model. The global LT-modip distribution map of the effective ionization parameter (Az) was estimated accordingly through this ingestion procedure, then the NeQuick 2 model could be driven by an Az map to reproduce ionospheric parameters, such as Ne, TEC, NmF2, hmF2, etc. In general, the performance of the Madrigal TEC-driven-NeQuick 2 can reduce the errors around 30-50% compared with those before data ingestion and it can capture more subtle ionospheric features. The accuracy of the ingestion results are further validated through comparison with various IGS GIMs, and the statistical analysis demonstrates that the data ingestion results have slightly lower RMSE (∼1 TECU) and bias than those of IGS GIMs. A further comparison with ionosonde data shows that the ability of NeQuick 2 to reproduce the foF2 is also improved after data ingestion. Moreover, the EOF technique is used to construct a time-dependent model of Az. The intrinsic diurnal variation and spatial distribution of the original data set can be well represented by EOF base functions, and 90% of the total variances can be well captured by using the fist 6 EOF series. The associated EOF coefficients can be expressed as a combination of 1) linear functions of $F_{10.7}$ and Ap index to show the dependence on solar/geomagnetic activity, and 2) a series of trigonometric functions with different periods to represent annual/seasonal variation components. In comparison with the Galileo ionospheric correction algorithm, the accuracy of TEC prediction by using the EOF modeled Az is improved to some extent (∼10-15%) though both results have large deviations for a short period during the storm recovery phase. These preliminary results indicate the effectiveness of this data ingestion and EOF modeling technique in bringing certain systematic improvement of ionosphere now-cast/forecast, while further modification could still be needed in the future to make this product more robust for both scientific study and space weather applications.

Acknowledgments. This work is sponsored by the National Key R&D Program of China (2016YFB0501503), National Science Foundation of China (41404125, 41674183), AFOSR under DDDAS (Dynamic Data-Driven applications Systems http://www.1dddas.org/) grant FA9550-16-1-0071, and Youth Innovation Promotion Association of Chinese Academy of Sciences. The authors acknowledges S. Radicella and B. Nava from Abdus Salam International Centre for Theoretical Physics (ICTP) in providing NeQuick 2 code. The ionosonde data are downloaded from NOAA Space Weather Prediction Center at: ftp.swpc.noaa.gov/pub/. The solar/geomagnetic activity indices data are obtained from the NASA Goddard Space Flight Center Coordinated Data Analysis Web. The IGS GIMs data are acquired from NASA's archive of space geodesy data: Crustal Dynamics Data Information System (CDDIS). GPS TEC data products and access through the Madrigal distributed data system are provided to the community by the Massachusetts Institute of Technology under support from US National Science Foundation grant AGS-1242204. Data for the TEC processing is provided from the following organizations: UNAVCO, Scripps Orbit and Permanent Array Center, Institut Geographique National, France, International GNSS Service, The Crustal Dynamics Data Information System (CDDIS), National Geodetic Survey, Instituto Brasileiro de Geografia e Estatística, RAMSAC CORS of Instituto Geográfico Nacional de la República Argentina, Arecibo Observatory, Low-Latitude Ionospheric Sensor Network (LISN), Topcon Positioning Systems, Inc., Canadian High Arctic Ionospheric Network, Institute of Geology and Geophysics, Chinese Academy of Sciences, China Meteorology Administration, Centro di Ricerche Sismologiche, Système d'Observation du Niveau des Eaux Littorales (SONEL), RENAG : REseau NAtional GPS permanent, GeoNet - the official source of geological hazard information for New Zealand, GNSS Reference Networks, Finnish Meteorological Institute, and SWEPOS - Sweden.

References

Aa, E., W. Huang, S. Yu, S. Liu, L. Shi, J. Gong, Y. Chen, and H. Shen (2015), A regional ionospheric TEC mapping technique over China and adjacent areas on the basis of data assimilation, *J. Geophys. Res. Space Physics*, *120*, 5049–5061, doi: 10.1002/2015JA021140.

Aa, E., S. Liu, W. Huang, L. Shi, J. Gong, Y. Chen, H. Shen, and J. Li (2016), Regional 3-D ionospheric electron density specification on the basis of data assimilation of ground-based GNSS and radio occultation data, *Space Weather*, *14*, 433–448, doi: 10.1002/2016SW001363.

Angling, M. J., and P. S. Cannon (2004), Assimilation of radio occultation measurements into background ionospheric models, *Radio Sci.*, *39*, RS1S08, doi: 10.1029/2002RS002819.

Angling, M. J., and B. Khattatov (2006), Comparative study of two assimilative models of the ionosphere, *Radio Sci.*, *41*, RS5S20, doi:10.1029/2005RS003372.

Bidaine, B., and R. Warnant (2011), Ionosphere modelling for Galileo single frequency users: Illustration of the combination of the NeQuick model and GNSS data ingestion, *Adv. Space Res.*, *47*, 312–322, doi:10.1016/j.asr.2010.09.001.

Bilitza, D. (2001), International Reference Ionosphere 2000, *Radio Sci.*, *36*(2), 261–275, doi:10.1029/2000rs002432.

Bilitza, D., and B. W. Reinisch (2008), International Reference Ionosphere 2007: Improvements and new parameters, *Adv. Space Res.*, *42*, 599–609, doi:10.1016/j.asr.2007.07.048.

Brunini, C., F. Azpilicueta, M. Gende, E. Camilion, A. A. Ángel, M. Hernandez-Pajares, M. Juan, J. Sanz, and D. Salazar (2011), Ground- and space-based GPS data ingestion into the NeQuick model, *J. Geod.*, *85*, 931–939, doi:10.1007/s00190-011-0452-4.

Bust, G. S., T. W. Garner, and T. L. Gaussiran (2004), Ionospheric Data Assimilation Three-Dimensional (IDA3D): A global, multisensor, electron density specification algorithm, *J. Geophys. Res.*, *109*, A11312, doi:10.1029/2003JA010234.

Bust, G. S., G. Crowley, T. W. Garner, T. L. Gaussiran, R. W. Meggs, C. N. Mitchell, P. S. J. Spencer, P. Yin, and B. Zapfe (2007), Four-dimensional GPS imaging of space weather storms, *Space Weather*, *5*, 02003, doi:10.1029/2006SW000237.

Coïsson, P., S. M. Radicella, R. Leitinger, and B. Nava (2006), Topside electron density in IRI and NeQuick: Features and limitations, *Adv. Space Res.*, *37*, 937–942, doi:10.1016/j.asr.2005.09.015.

Di Giovanni, G., and S. M. Radicella (1990), An analytical model of the electron density profile in the ionosphere, *Adv. Space Res.*, *10*, 27–30, doi:10.1016/0273-1177(90)90301-F.

Dvinskikh, N. I. (1988), Expansion of ionospheric characteristics fields in empirical orthogonal functions, *Adv. Space Res.*, *8*, 179–187, doi:10.1016/0273-1177(88)90238-4.

Feltens, J. (2007), Development of a new three-dimensional mathematical ionosphere model at European Space Agency/European Space Operations Centre, *Space Weather*, *5*, S12,002, doi:10.1029/2006SW000294.

Feltens, J., and S. Schaer (1998), IGS Products for the Ionosphere, IGS Position Paper, in *the IGS analysis centers workshop*, pp. 225–232, Darmstadt, Germany.

Fuller-Rowell, T., E. Araujo-Pradere, C. Minter, M. Codrescu, P. Spencer, D. Robertson, and A. R. Jacobson (2006), US-TEC: A new data assimilation product from the Space Environment Center characterizing the ionospheric total electron content using real-time GPS data, *Radio Sci.*, *41*, RS6003, doi:10.1029/2005RS003393.

Galkin, I. A., B. W. Reinisch, X. Huang, and D. Bilitza (2012), Assimilation of GIRO data into a real-time IRI, *Radio Sci.*, *47*, RS0L07, doi:10.1029/2011RS004952.

Hernández-Pajares, M., J. M. Juan, and J. Sanz (1999), New approaches in global ionospheric determination using ground GPS data, *J. Atmos. Sol-Terr. Phys.*, *61*, 1237–1247, doi:10.1016/S1364-6826(99)00054-1.

Hernández-Pajares, M., J. M. Juan, J. Sanz, R. Orus, A. Garcia-Rigo, J. Feltens, A. Komjathy, S. C. Schaer, and A. Krankowski (2009), The IGS VTEC maps: a reliable source of ionospheric information since 1998, *J. Geod.*, *83*, 263–275, doi:10.1007/s00190-008-0266-1.

Jolliffe, I. T. (1990), Principal component analysis: A beginner's guide - I. Introduction and application, *Weather*, *45*, 375–382, doi:10.1002/j.1477-8696.1990.tb05558.x.

Komjathy, A., L. Sparks, B. D. Wilson, and A. J. Mannucci (2005), Automated daily processing of more than 1000 ground-based GPS receivers for studying intense ionospheric storms, *Radio Sci.*, *40*, RS6006, doi:10.1029/2005RS003279.

Komjathy, A., B. Wilson, X. Pi, V. Akopian, M. Dumett, B. Iijima, O. Verkhoglyadova, and A. J. Mannucci (2010), JPL/USC GAIM: On the impact of using COSMIC and ground-based GPS measurements to estimate ionospheric parameters, *J. Geophys. Res.*, *115*, A02307, doi:10.1029/2009JA014420.

Lee, I. T., T. Matsuo, A. D. Richmond, J. Y. Liu, W. Wang, C. H. Lin, J. L. Anderson, and M. Q. Chen (2012), Assimilation of FORMOSAT-3/COSMIC electron density profiles into a coupled thermosphere/ionosphere model using ensemble Kalman filtering, *J. Geophys. Res.*, *117*, A10318, doi:10.1029/2012JA017700.

Leitinger, R., M. Zhang, and S. M. Radicella (2005), An improved bottomside for the ionospheric electron density model nequick, *Ann. Geophys.*, *48*(3), doi:10.4401/ag-3217.

Li, Z., Y. Yuan, N. Wang, M. Hernandez-Pajares, and X. Huo (2015), SHPTS: towards a new method for generating precise global ionospheric TEC map based on spherical harmonic and generalized trigonometric series functions, *J. Geod.*, *89*, 331–345, doi:10.1007/s00190-014-0778-9.

Mandrake, L., B. Wilson, C. Wang, G. Hajj, A. Mannucci, and X. Pi (2005), A performance evaluation of the operational Jet Propulsion Laboratory/University of Southern California Global Assimilation Ionospheric Model (JPL/USC GAIM), *J. Geophys. Res.*, *110*, A12306, doi:10.1029/2005JA011170.

Mannucci, A. J., B. D. Wilson, D. N. Yuan, C. H. Ho, U. J. Lindqwister, and T. F. Runge (1998), A global mapping technique for GPS-derived ionospheric total electron content measurements, *Radio Sci.*, *33*, 565–582, doi:10.1029/97RS02707.

Matsuo, T., M. Fedrizzi, T. J. Fuller-Rowell, and M. V. Codrescu (2012), Data assimilation of thermospheric mass density, *Space Weather*, *10*, 05002, doi:10.1029/2012SW000773.

Nava, B., P. Coïsson, G. Miró Amarante, F. Azpilicueta, and S. M. Radicella (2005), A model assisted ionospheric electron density reconstruction method based on vertical tec data ingestion, *Ann. Geophys.*, *48*(2), doi:10.4401/ag-3203.

Nava, B., S. M. Radicella, R. Leitinger, and P. Coïsson (2006), A near-real-time model-assisted ionosphere electron density retrieval method, *Radio Sci.*, *41*, RS6S16, doi:10.1029/2005RS003386.

Nava, B., P. Coïsson, and S. M. Radicella (2008), A new version of the NeQuick ionosphere electron density model, *J. Atmos. Sol. Terr. Phys*, *70*, 1856–1862, doi:

10.1016/j.jastp.2008.01.015.

Nava, B., S. M. Radicella, and F. Azpilicueta (2011), Data ingestion into NeQuick 2, *Radio Sci.*, *46*, RS0D17, doi:10.1029/2010RS004635.

Nigussie, M., S. M. Radicella, B. Damtie, E. Yizengaw, B. Nava, and L. Roininen (2016), Validation of NeQuick TEC data ingestion technique against C/NOFS and EISCAT electron density measurements, *Radio Sci.*, *51*, 905–917, doi:10.1002/2015RS005930.

Pi, X., C. Wang, G. A. Hajj, G. Rosen, B. D. Wilson, and G. J. Bailey (2003), Estimation of E×B drift using a global assimilative ionospheric model: An observation system simulation experiment, *J. Geophys. Res.*, *108*, 1075, doi:10.1029/2001JA009235.

Pi, X., A. J. Mannucci, B. A. Iijima, B. D. Wilson, A. Komjathy, T. F. Runge, and V. Akopian (2009), Assimilative modeling of ionospheric disturbances with FORMOSAT-3/COSMIC and ground-based GPS measurements, *Terr. Atmos. Ocean. Sci.*, *20*.

Radicella, S. M., and R. Leitinger (2001), The evolution of the DGR approach to model electron density profiles, *Adv. Space Res.*, *27*, 35–40, doi:10.1016/S0273-1177(00)00138-1.

Rawer, K. (1963), Propagation of decameter waves (HF band), in *Meteorological and Astronomical Influences on Radio Wave Propogation*, edited by B. Landmark, pp. 221–250.

Rideout, W., and A. Coster (2006), Automated gps processing for global total electron content data, *GPS Solut.*, *10*(3), 219–228, doi:10.1007/s10291-006-0029-5.

Schaer, S. (1999), Mapping and predicting the Earth's ionosphere using the Global Positioning System., *Geod.-Geophys. Arb. Schweiz*, *59*.

Scherliess, L., R. W. Schunk, J. J. Sojka, and D. C. Thompson (2004), Development of a physics-based reduced state Kalman filter for the ionosphere, *Radio Sci.*, *39*, RS1S04, doi:10.1029/2002RS002797.

Scherliess, L., R. W. Schunk, J. J. Sojka, D. C. Thompson, and L. Zhu (2006), Utah State University Global Assimilation of Ionospheric Measurements Gauss-Markov Kalman filter model of the ionosphere: Model description and validation, *J. Geophys. Res.*, *111*, A11315, doi:10.1029/2006JA011712.

Schunk, R. W., L. Scherliess, J. J. Sojka, D. C. Thompson, D. N. Anderson, M. Codrescu, C. Minter, T. J. Fuller-Rowell, R. A. Heelis, M. Hairston, and B. M. Howe (2004), Global Assimilation of Ionospheric Measurements (GAIM), *Radio Sci.*, *39*, RS1S02, doi:10.1029/2002RS002794.

Schunk, R. W., L. Scherliess, J. J. Sojka, D. Thompson, and L. Zhu (2005), Ionospheric weather forecasting on the horizon, *Space Weather*, *3*, S08007, doi: 10.1029/2004SW000138.

Schunk, R. W., L. Scherliess, V. Eccles, L. C. Gardner, J. J. Sojka, L. Zhu, X. Pi, A. J. Mannucci, B. D. Wilson, A. Komjathy, C. Wang, and G. Rosen (2014), Ensemble Modeling with Data Assimilation Models: A New Strategy for Space Weather Specifications, Forecasts, and Science, *Space Weather*, *12*, 123–126, doi:10.1002/2014SW001050.

Singer, W., and N. I. Dvinskikh (1991), Comparison of empirical models of ionospheric characteristics developed by means of different mapping methods, *Adv. Space Res.*, *11*, 3–6, doi:10.1016/0273-1177(91)90311-7.

Vierinen, J., A. J. Coster, W. C. Rideout, P. J. Erickson, and J. Norberg (2016), Statistical framework for estimating GNSS bias, *Atmospheric Measurement Techniques*, *9*, 1303–

1312, doi:10.5194/amt-9-1303-2016.

Wang, C., G. Hajj, X. Pi, I. G. Rosen, and B. Wilson (2004), Development of the Global Assimilative Ionospheric Model, *Radio Sci.*, *39*, RS1S06, doi:10.1029/2002RS002854.

Yu, X., W. Zhen, B. Xiong, C. She, M. Ou, J. Xu, and D. Liu (2015), The performance of ionospheric correction based on NeQuick 2 model adaptation to Global Ionospheric Maps, *Adv. Space Res.*, *55*, 1741–1747, doi:10.1016/j.asr.2015.01.011.

Yue, X., W. S. Schreiner, Y.-C. Lin, C. Rocken, Y.-H. Kuo, and B. Zhao (2011), Data assimilation retrieval of electron density profiles from radio occultation measurements, *J. Geophys. Res.*, *116*, A03317, doi:10.1029/2010JA015980.

Yue, X., W. S. Schreiner, Y.-H. Kuo, D. C. Hunt, W. Wang, S. C. Solomon, A. G. Burns, D. Bilitza, J.-Y. Liu, W. Wan, and J. Wickert (2012), Global 3-D ionospheric electron density reanalysis based on multisource data assimilation, *J. Geophys. Res.*, *117*, A09325, doi:10.1029/2012JA017968.

Zhu, L., R. Schunk, L. Scherliess, and V. Eccles (2012), Importance of data assimilation technique in defining the model drivers for the space weather specification of the high-latitude ionosphere, *Radio Sci.*, *47*, RS0L24, doi:10.1029/2011RS004936.

Table 1. Variances of the first 6 EOF series.

EOF Series	Variances (%)	Cumulative Variances (%)
EOF 1	76.11	76.11
EOF 2	6.18	82.29
EOF 3	3.75	86.04
EOF 4	2.74	88.78
EOF 5	1.70	90.48
EOF 6	1.29	91.77

Table 2. Correlation of the first 6 EOF coefficients with respect to $F_{10.7}$ and Ap index.

Correlation	$F_{10.7}$	Ap
Coef 1	-0.96	-0.31
Coef 2	0.01	0.36
Coef 3	0.11	-0.08
Coef 4	0.10	0.27
Coef 5	0.08	0.49
Coef 6	-0.06	0.16

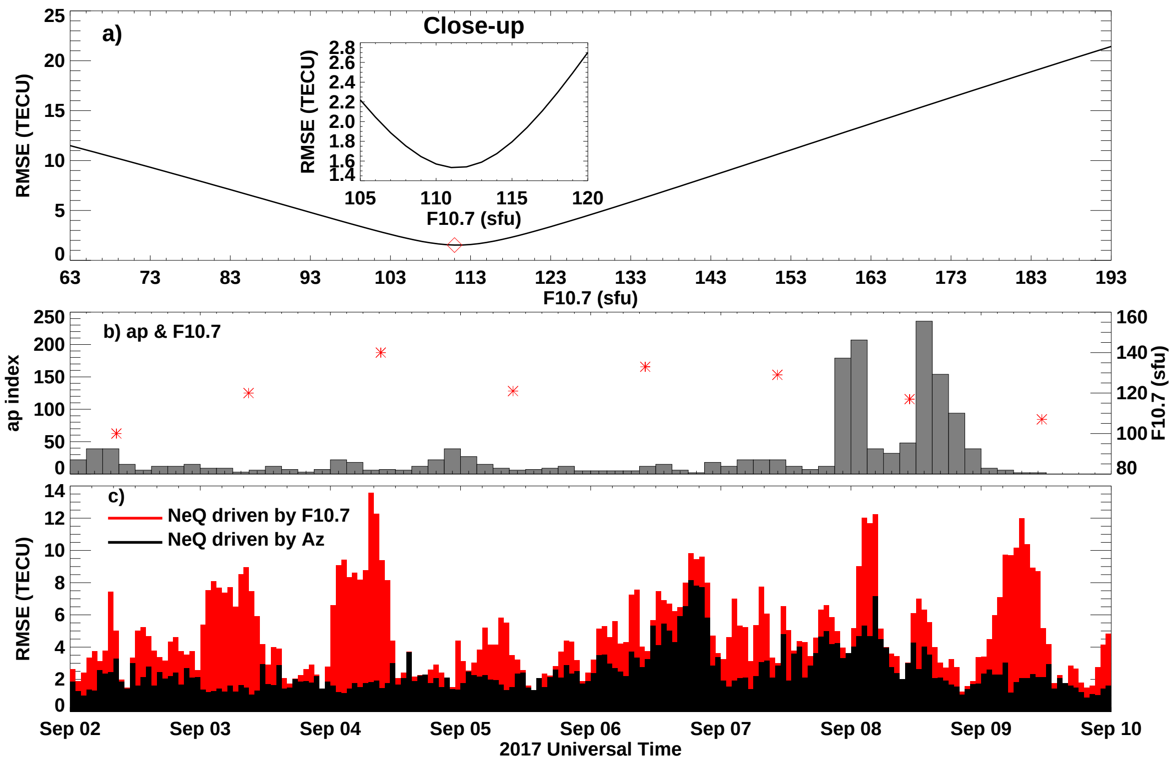

Figure 1. (a) A schematic diagram of RMSE variation with respect to $F_{10.7}$. The minimum error that corresponds to Az is marked with a diamond. (b) Temporal variation of ap index and $F_{10.7}$ during September 02-10, 2017. (c) An example of RMSE comparison between NeQuick 2 driven by $F_{10.7}$ (red) and driven by Az (black) at BJFS station (39.4°N, 115.9°E) during this interval.

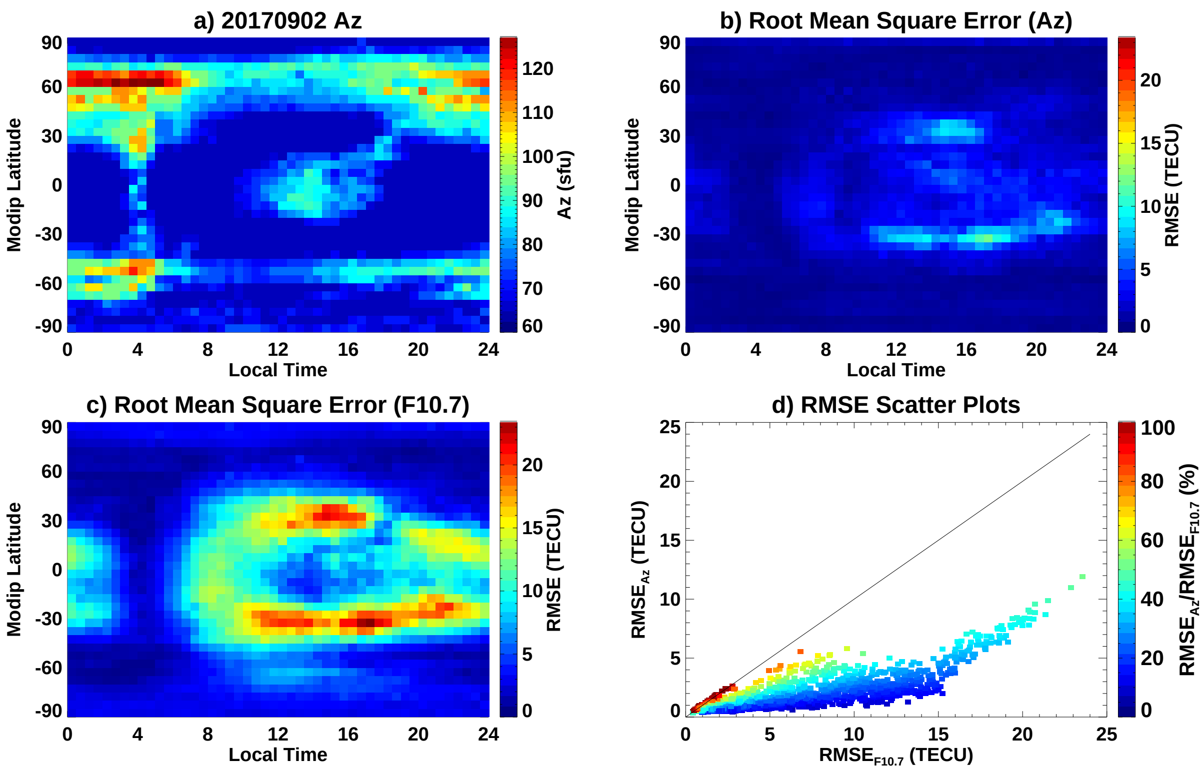

Figure 2. (a) An example of Modip-LT distribution of Az on September 02, 2017 after ingesting Madrigal TEC into NeQuick 2 model. (b) Distribution of RMSE after data ingestion. (c) Distribution of RMSE before data ingestion. (d) Scatter plot of RMSE$_{Az}$ versus RMSE$_{F10.7}$, while the color represent the ratio of RMSE after and before data ingestion.

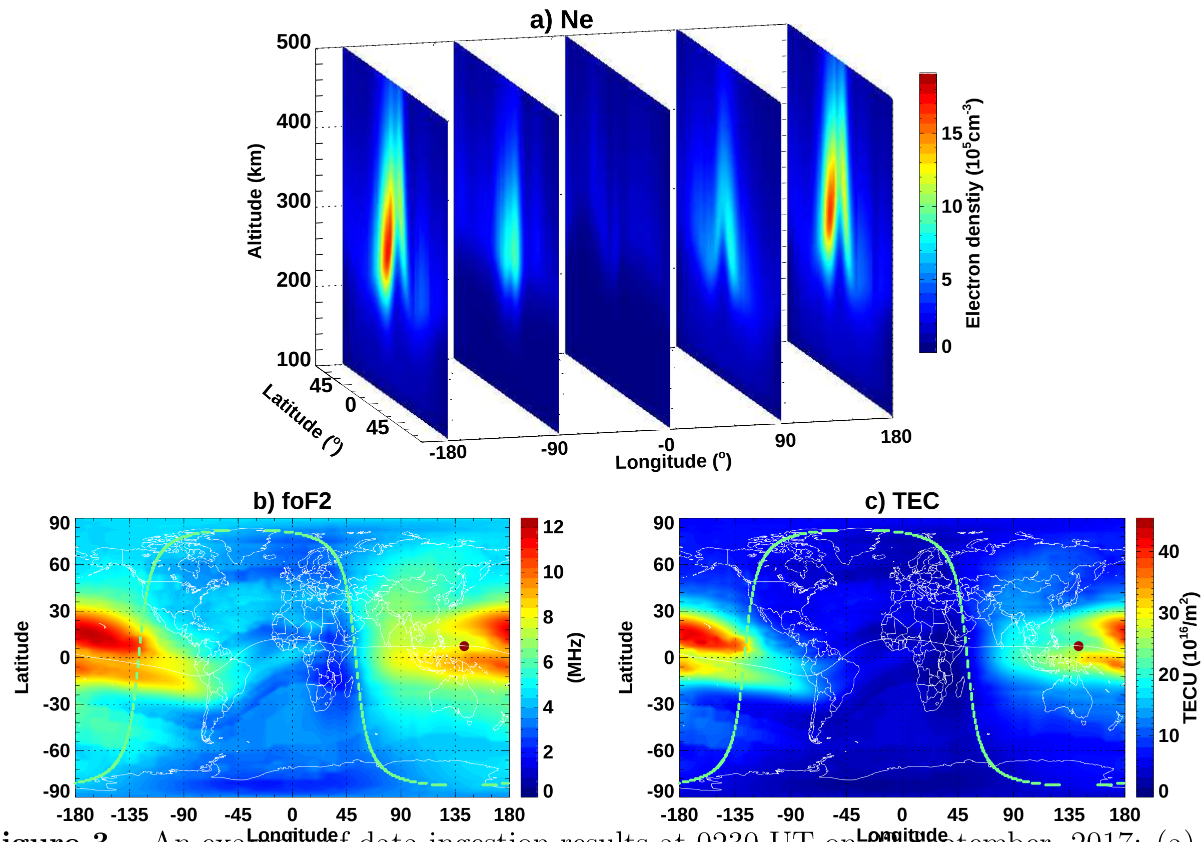

Figure 3. An example of data ingestion results at 0230 UT on 02 September, 2017: (a) global 3D electron density distribution; (b) F2 layer critical frequency (foF2); (c) vertical TEC map. The terminator, subsolar point, and geomagnetic equator are also marked in the maps.

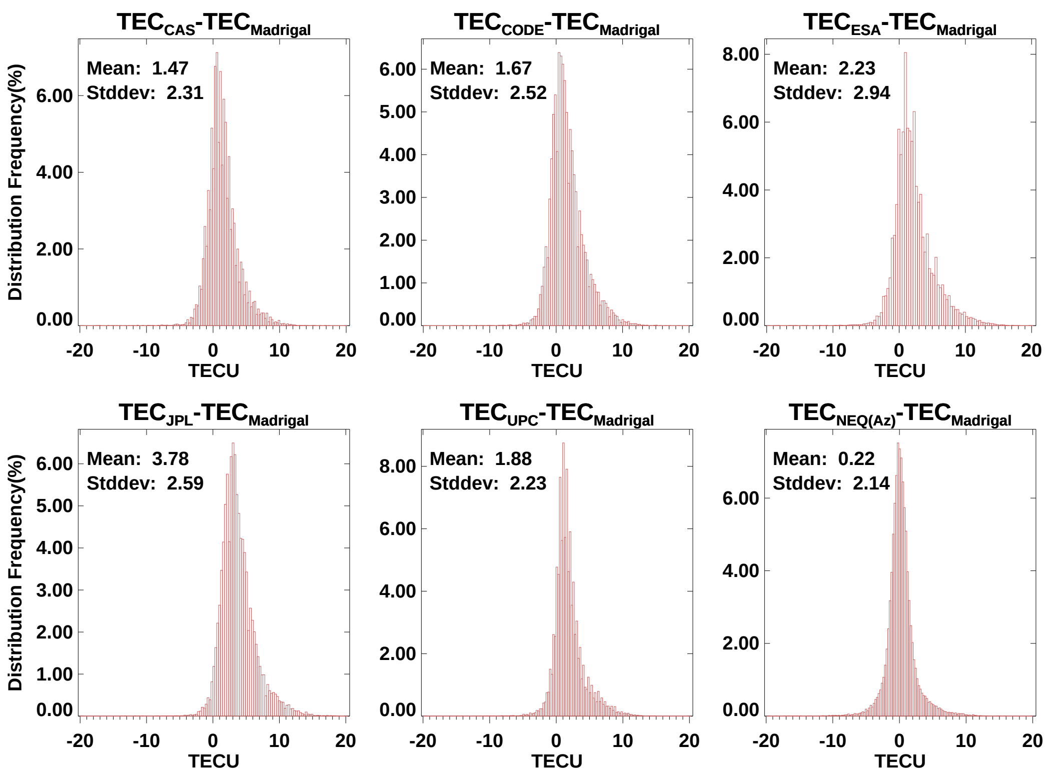

Figure 4. Histogram comparison of data ingestion results and IGS GIMs with respect to Madrigal TEC on 02 September 2017.

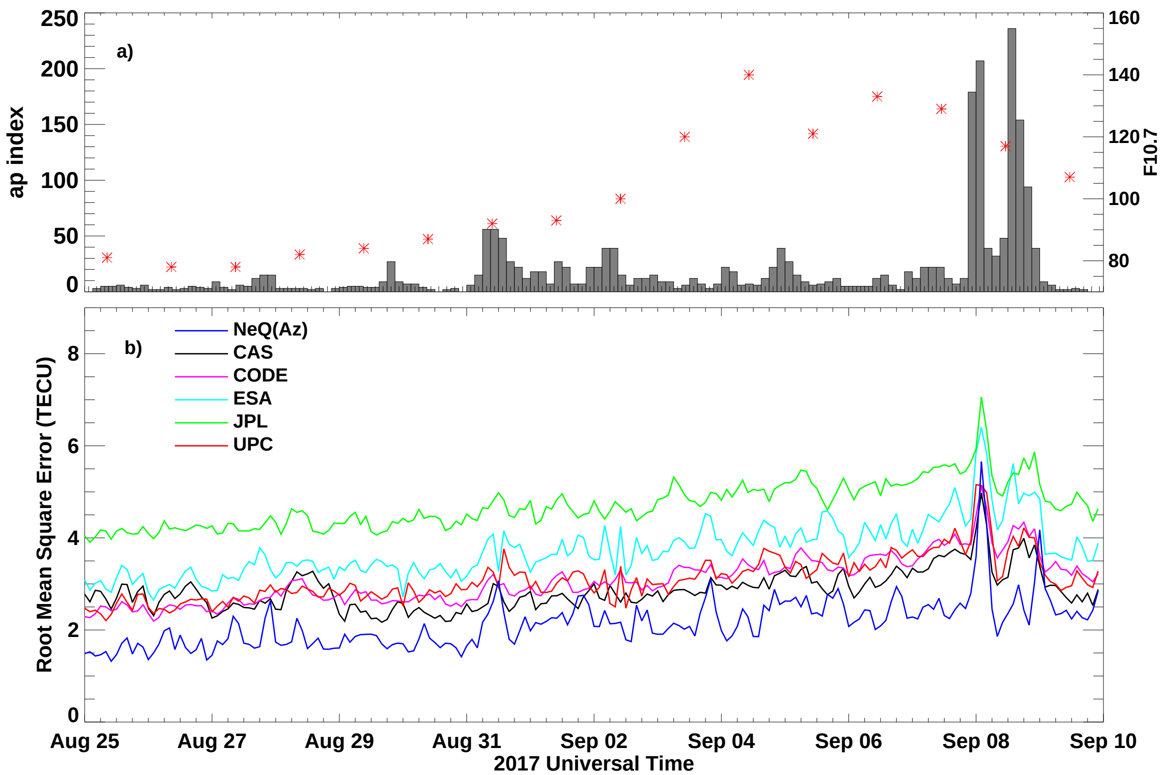

Figure 5. (a) Temporal variation of ap index and $F_{10.7}$ from August 25 to September 10, 2017. (b) RMSE variation for different TEC GIMs and NeQuick 2 driven by Az.

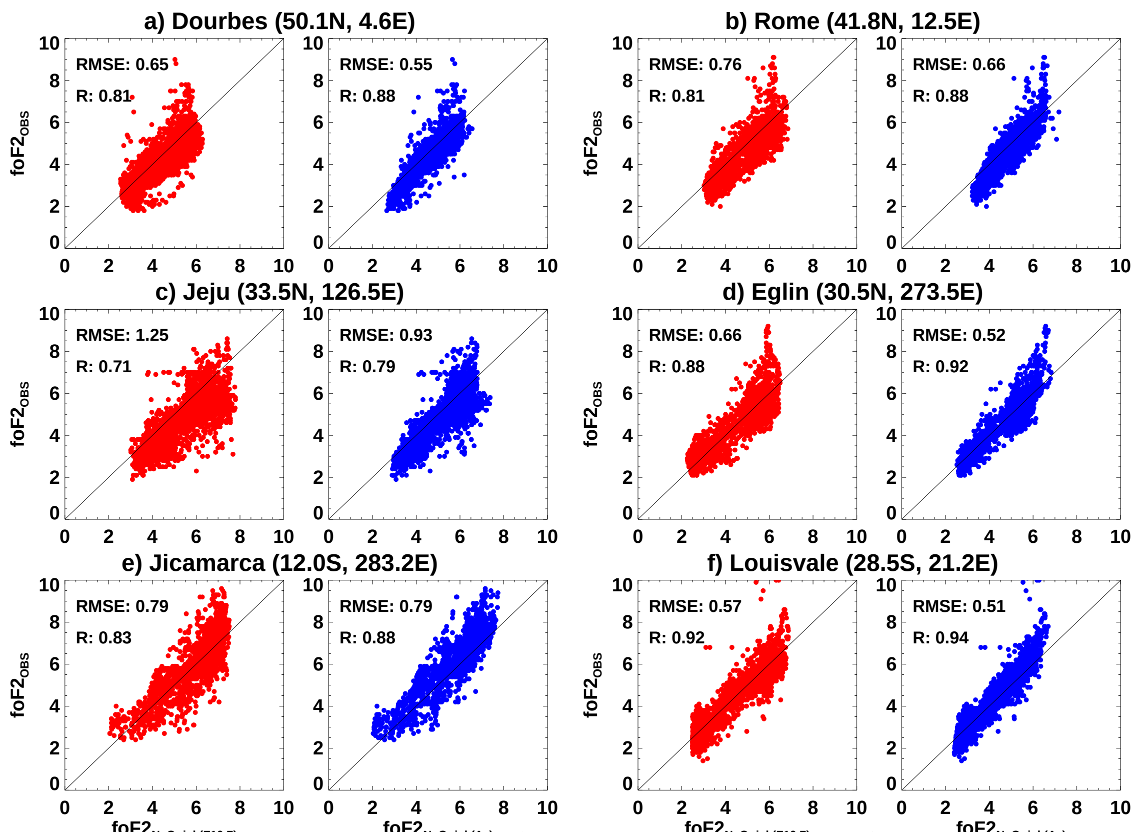

Figure 6. Scatter points comparison of ionosonde foF2 with NeQuick 2 driven by $F_{10.7}$ (red) and Az (blue) at 6 ionosonde stations.

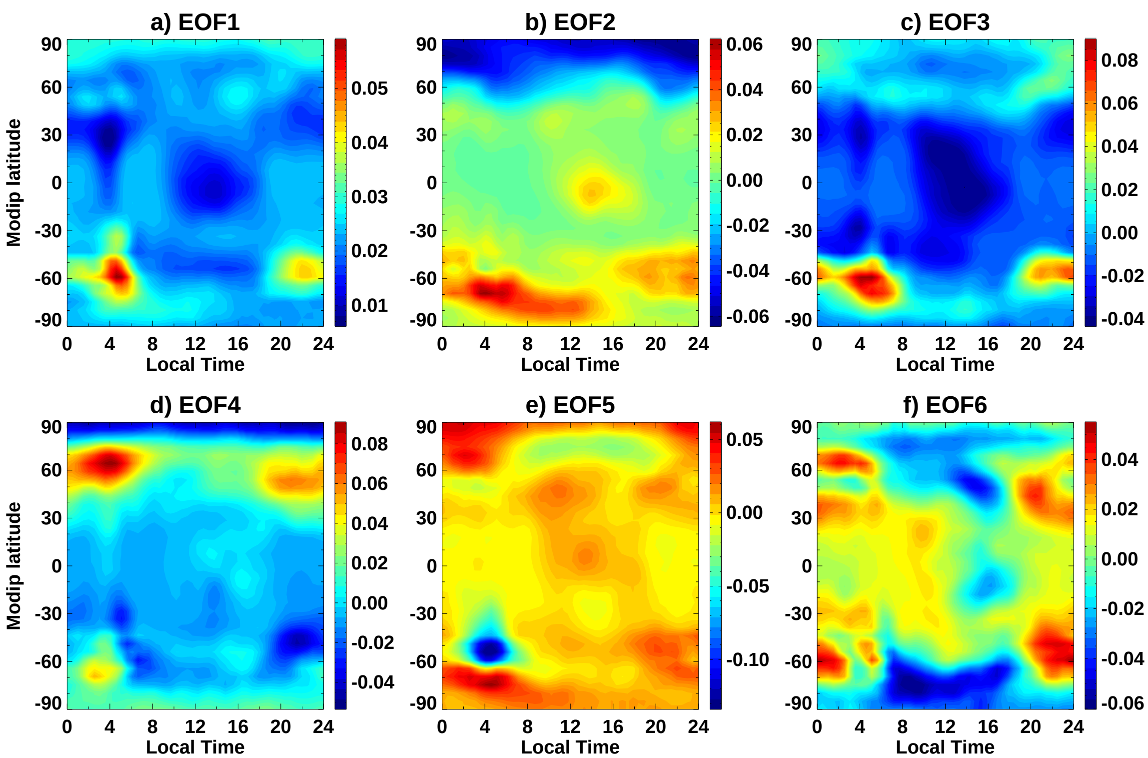

Figure 7. The modip latitude and local time distribution of the first 6 EOF base functions through decomposition of $Az/F_{10.7}$.

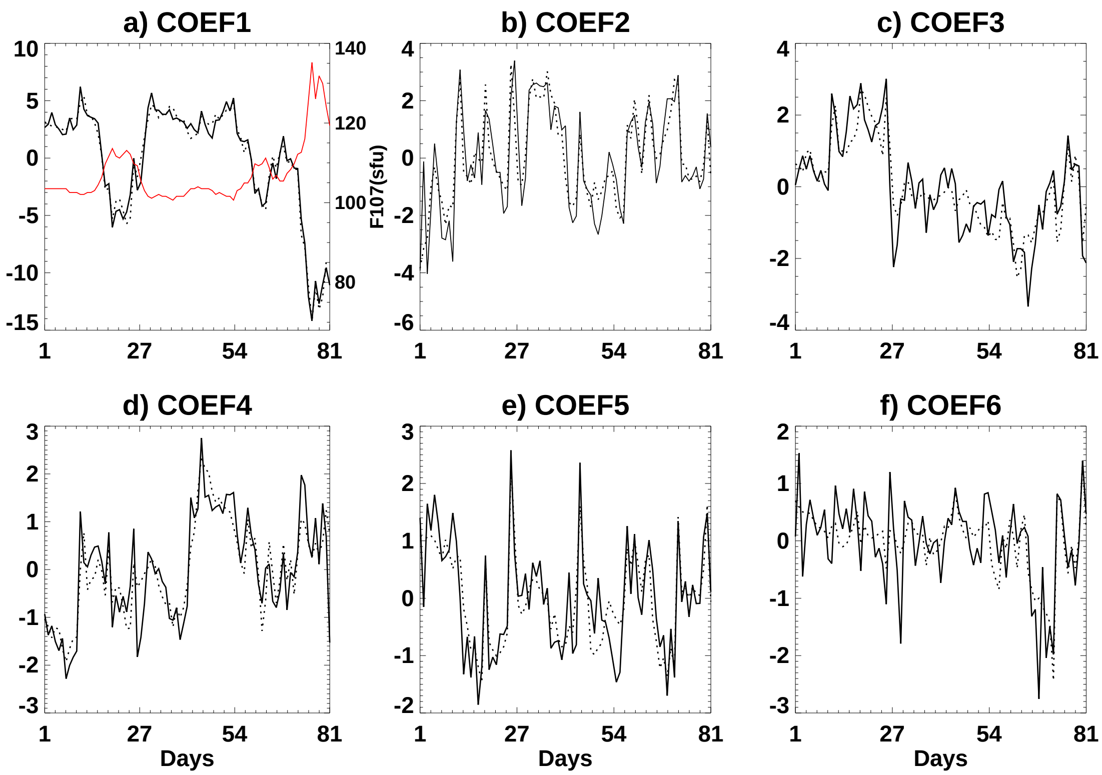

Figure 8. Temporal variation of the first 6 EOF coefficients through decomposition of $Az/F_{10.7}$. The observational $F_{10.7}$ (red) and modeled coefficients (dashed) are also marked.

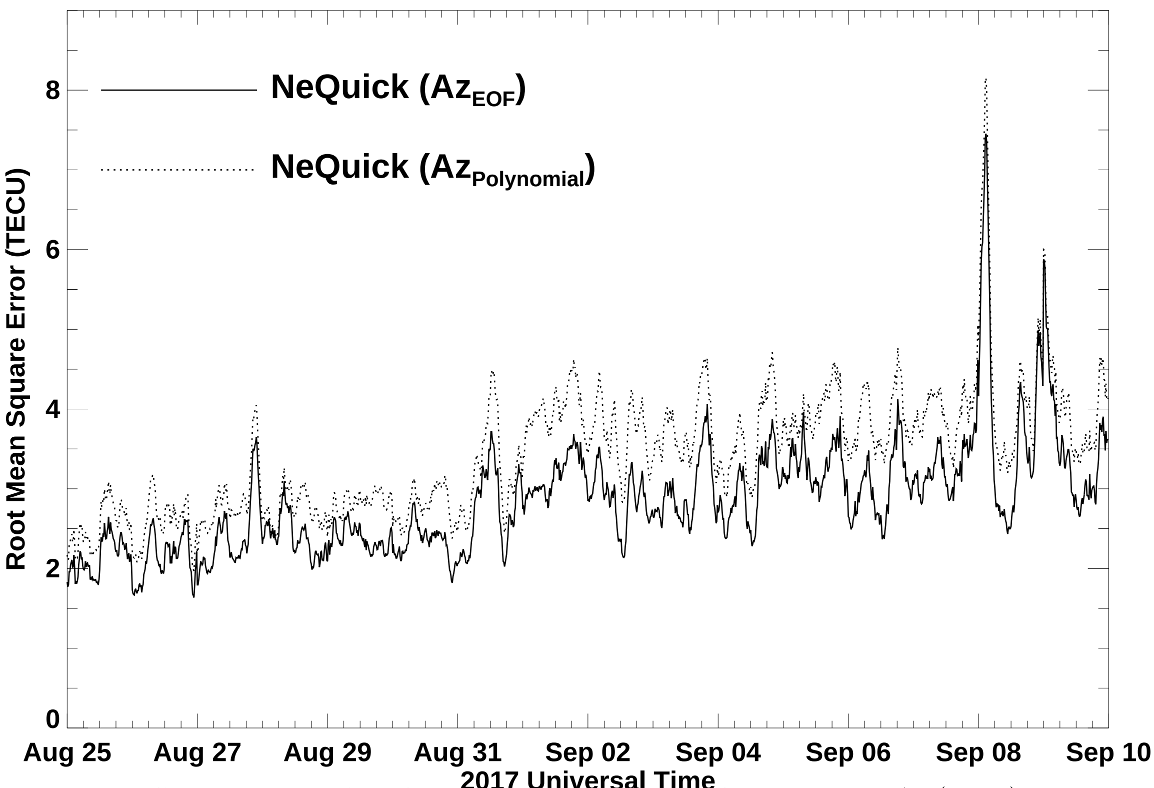

Figure 9. RMSE variation of NeQuick TEC driven by EOF modeled Az (solid) and polynomial fitted Az (dashed) during the time period from August 25 to September 10, 2017.

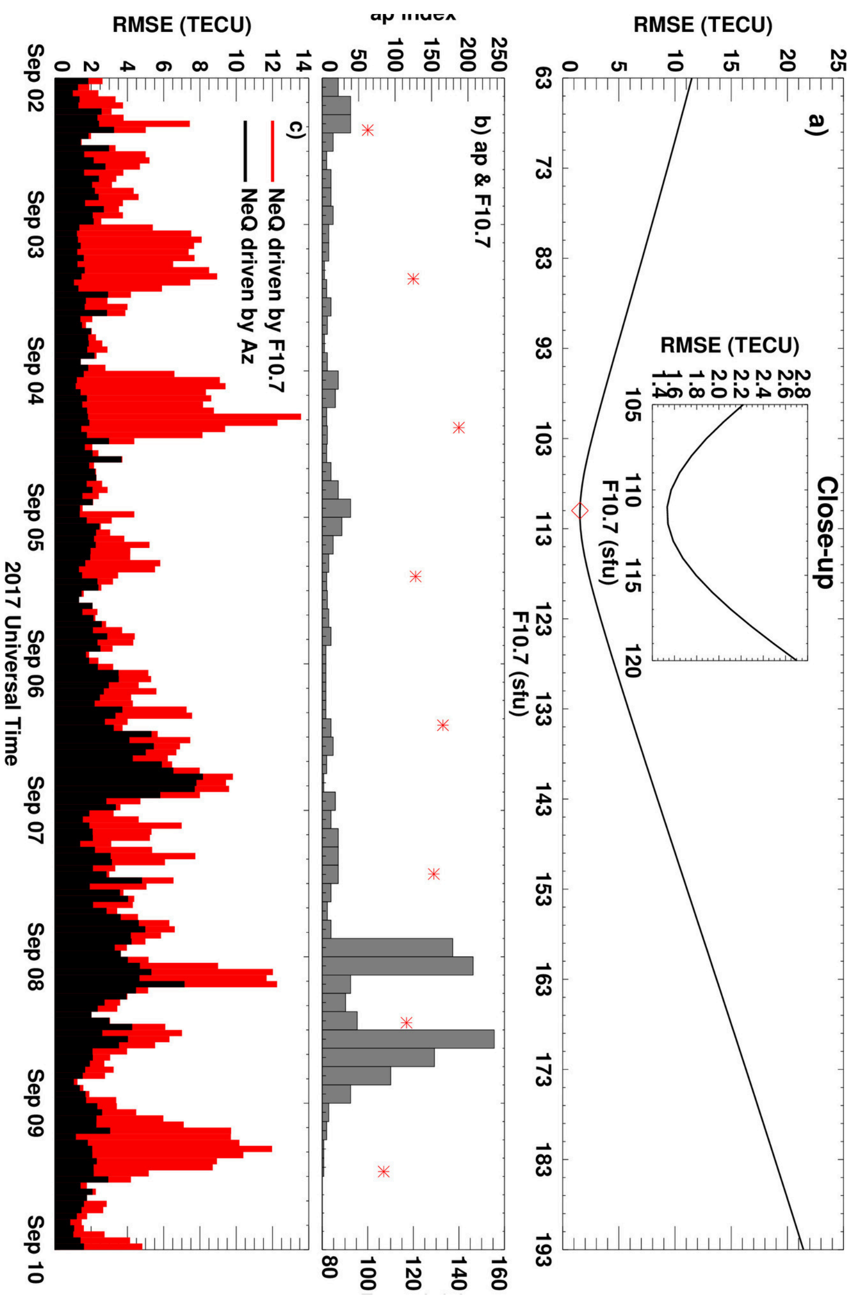

2018sw001987-f01-z-.eps

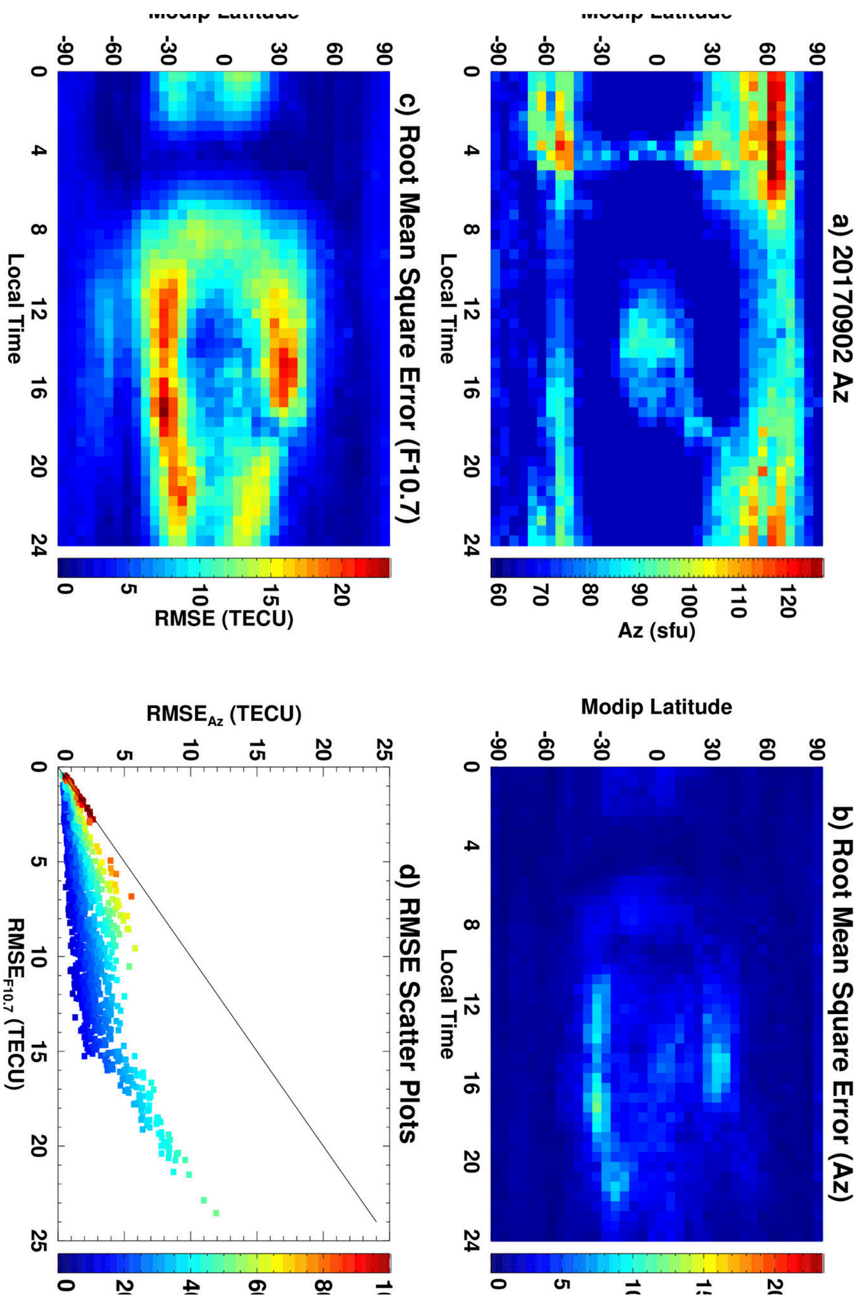

2018sw001987-f02-z-.eps

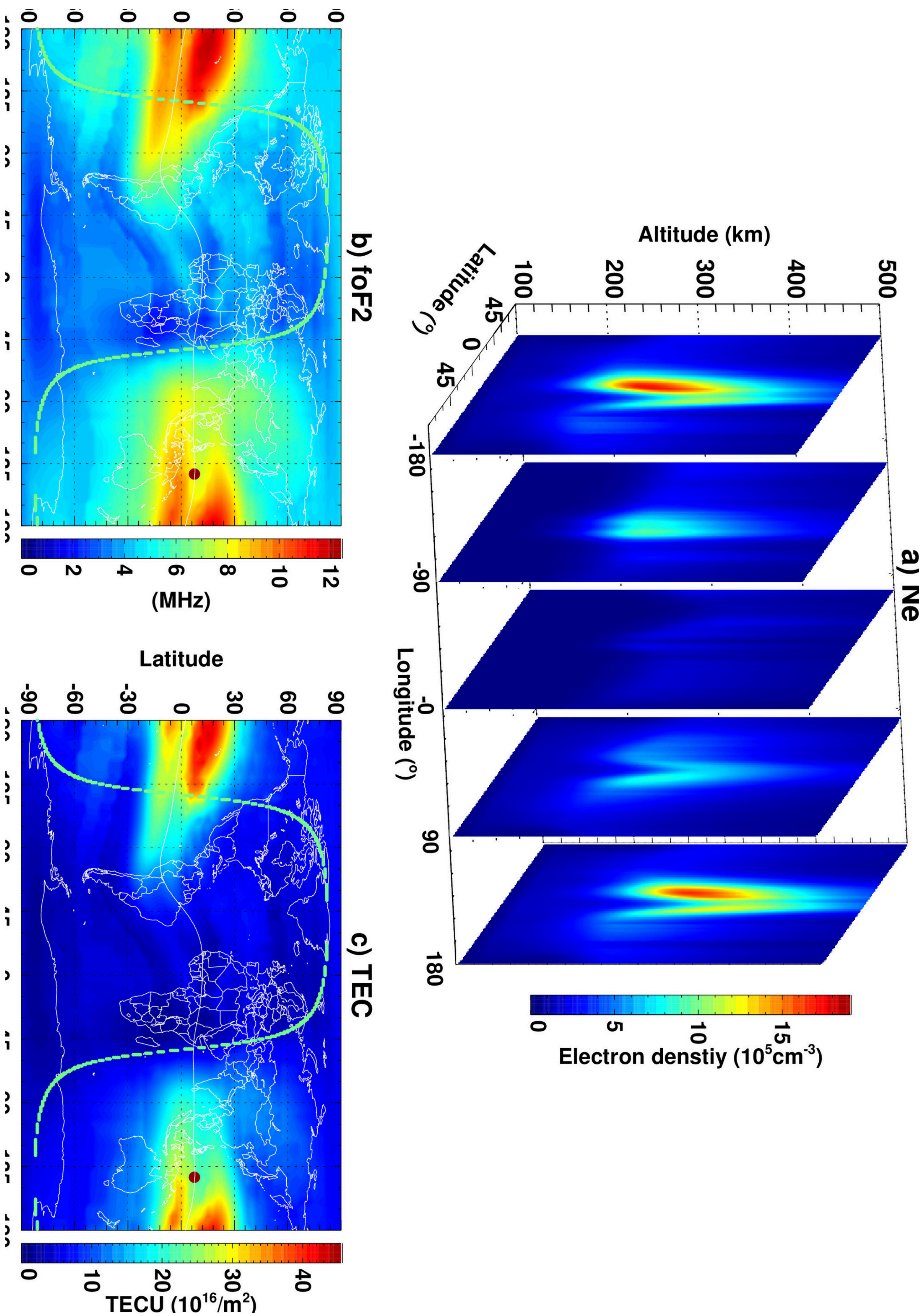

2018sw001987-f03-z-.eps

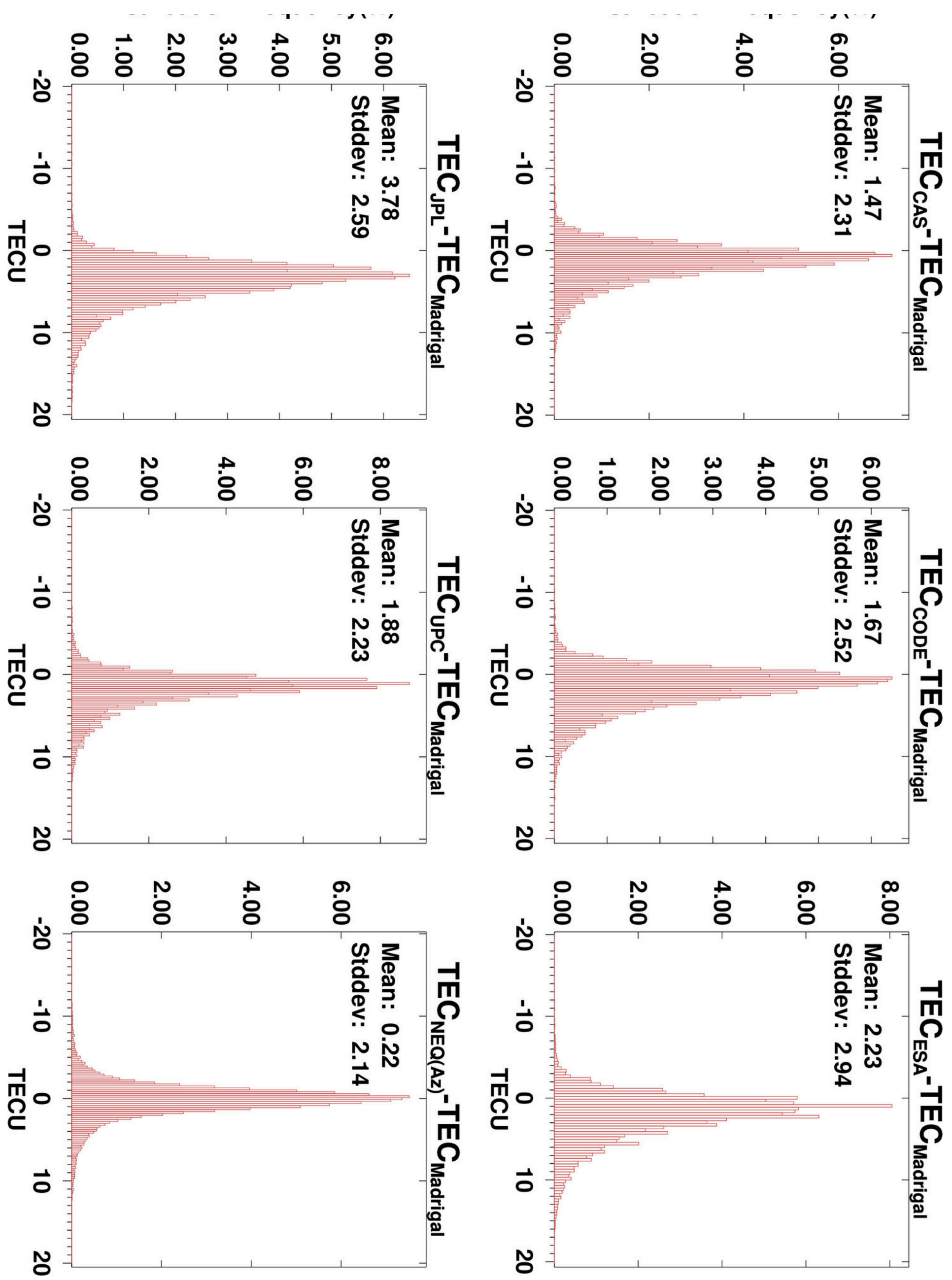

2018sw001987-f04-z-.eps

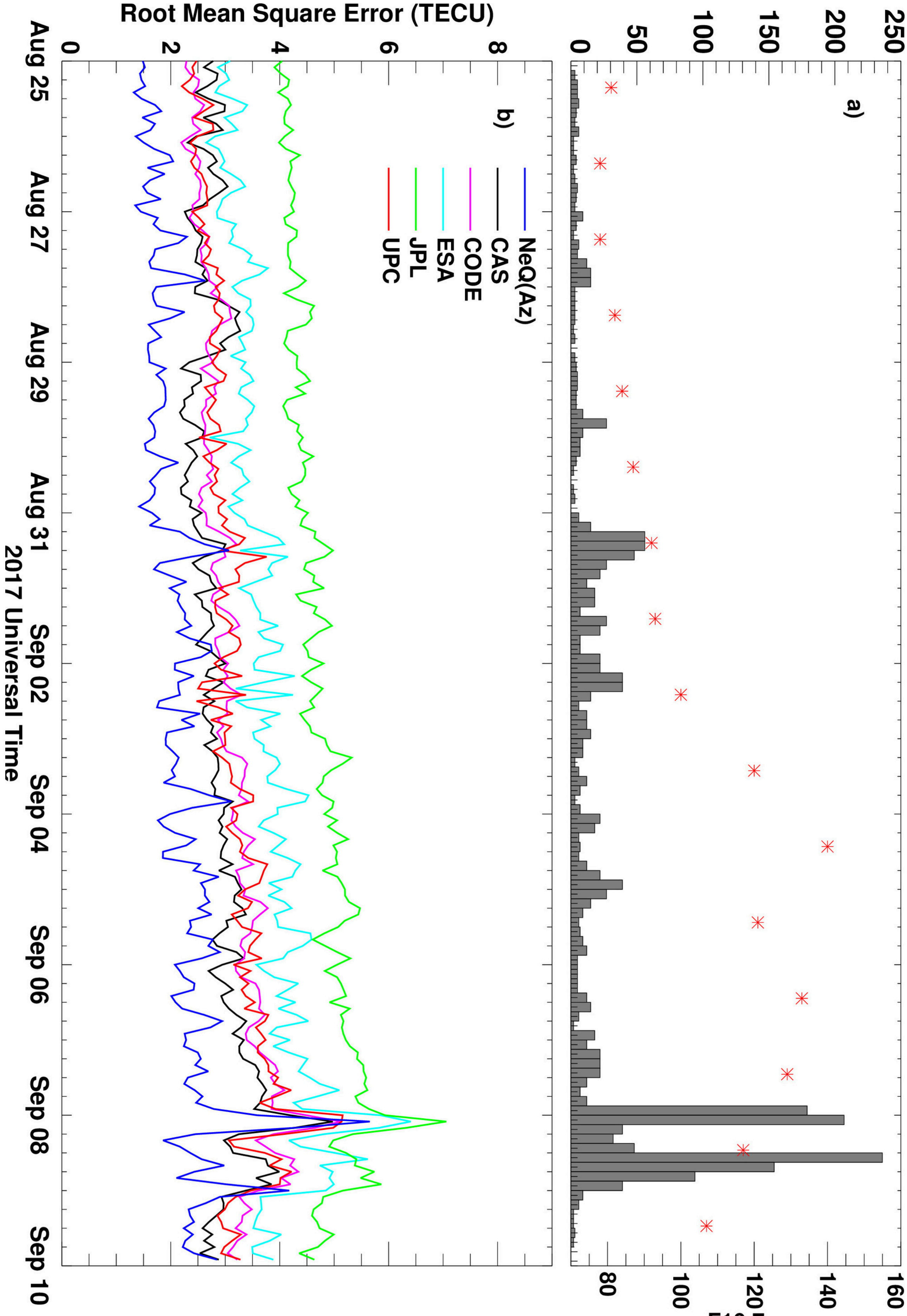

2018sw001987-f05-z-.eps

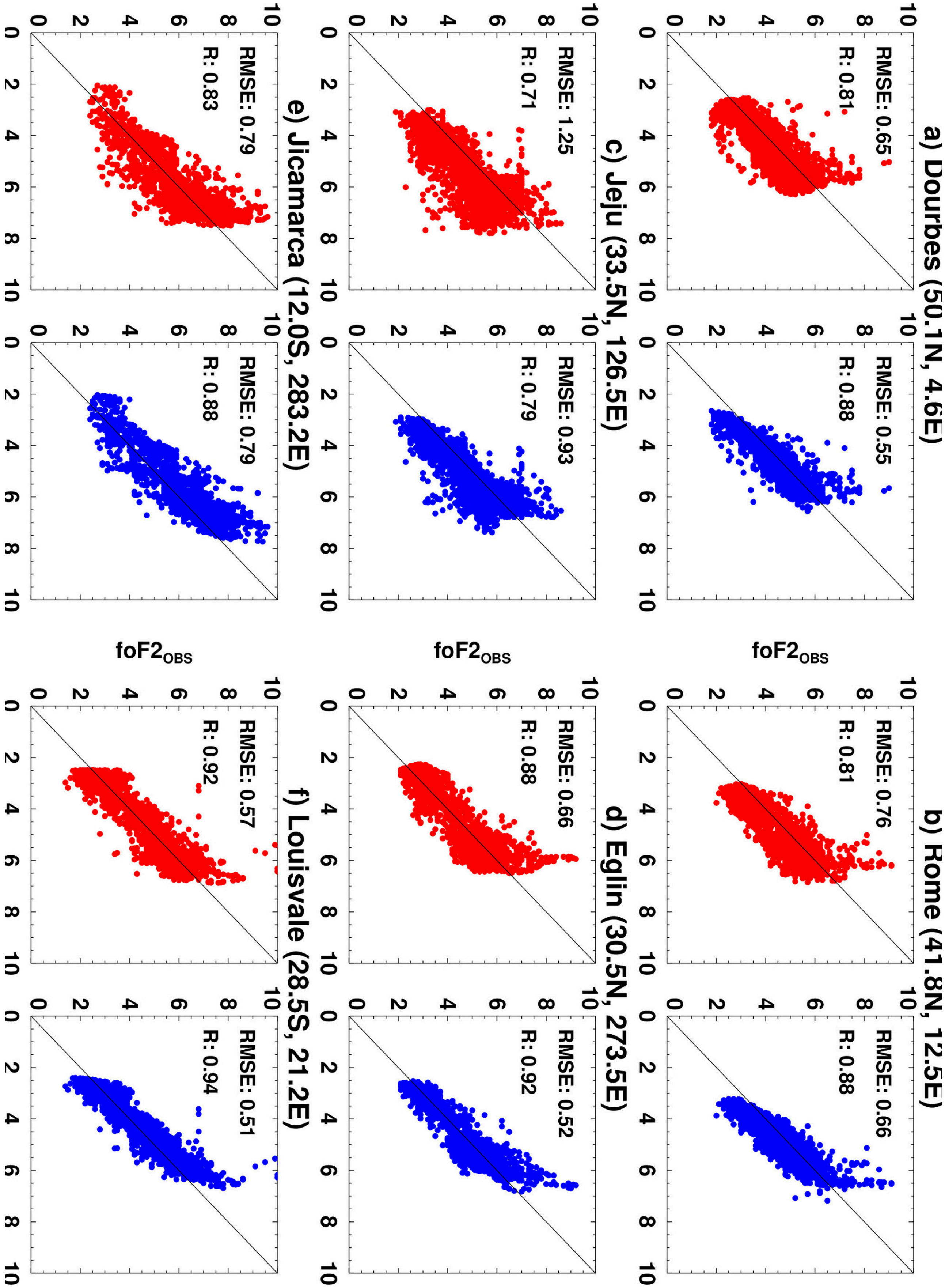

2018sw001987-f06-z-.eps

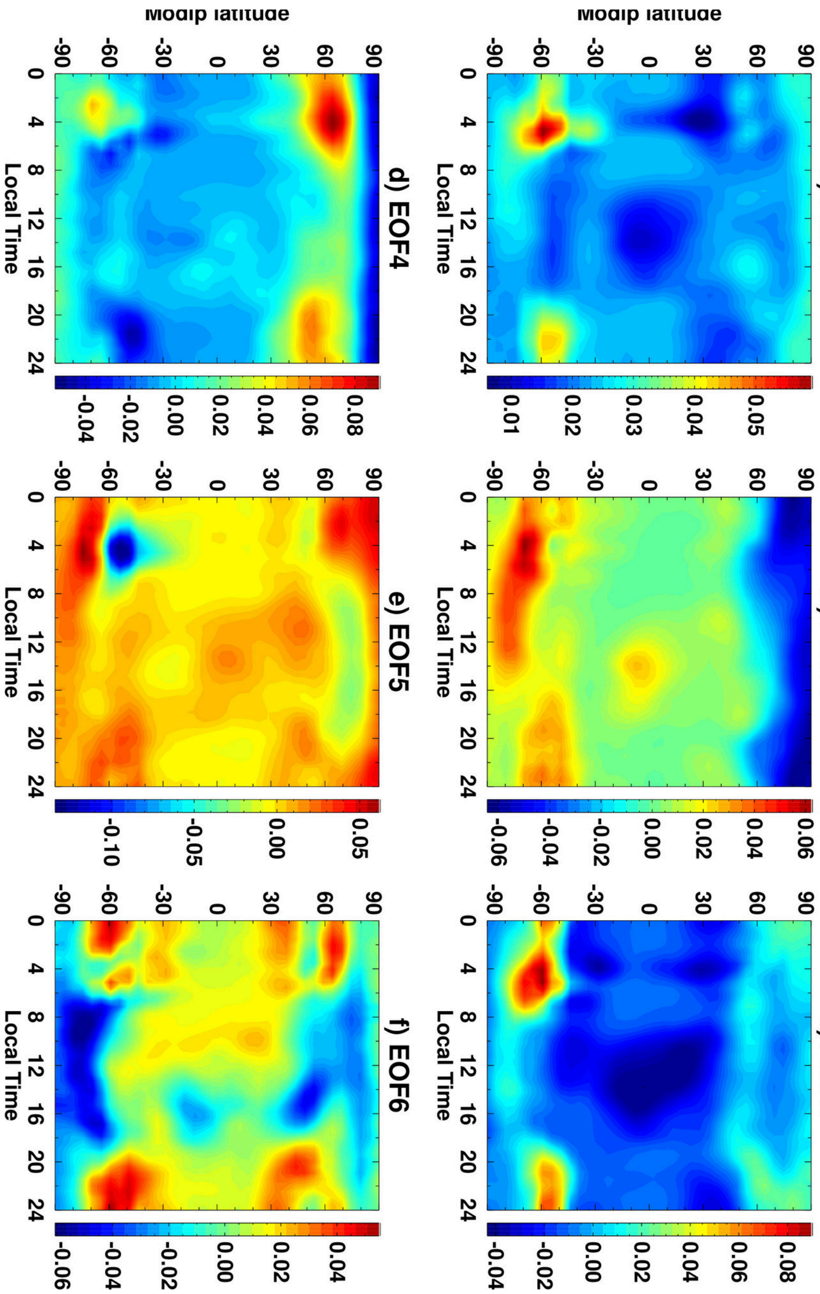

2018sw001987-f07-z-.eps

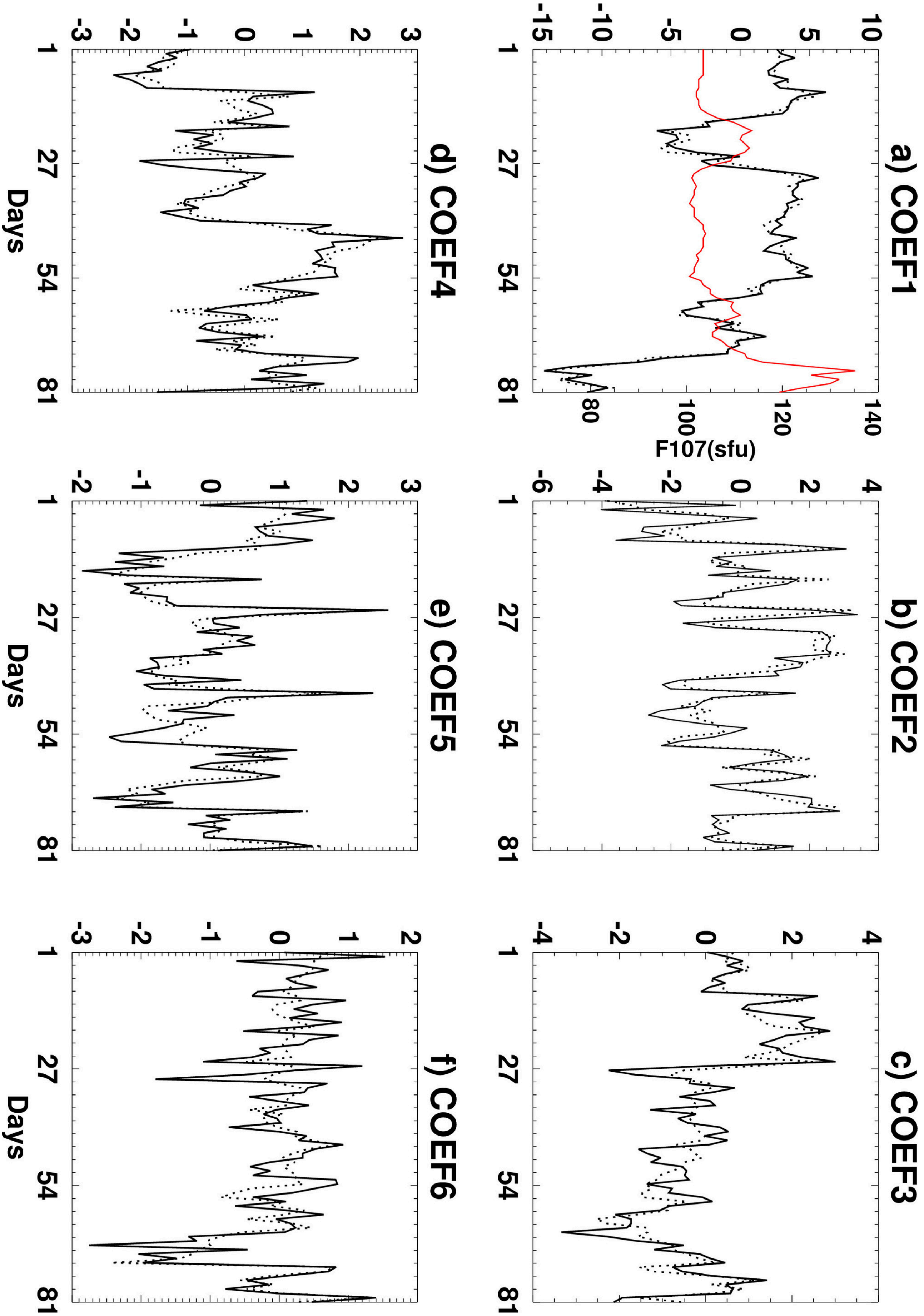

2018sw001987-f08-z-.eps

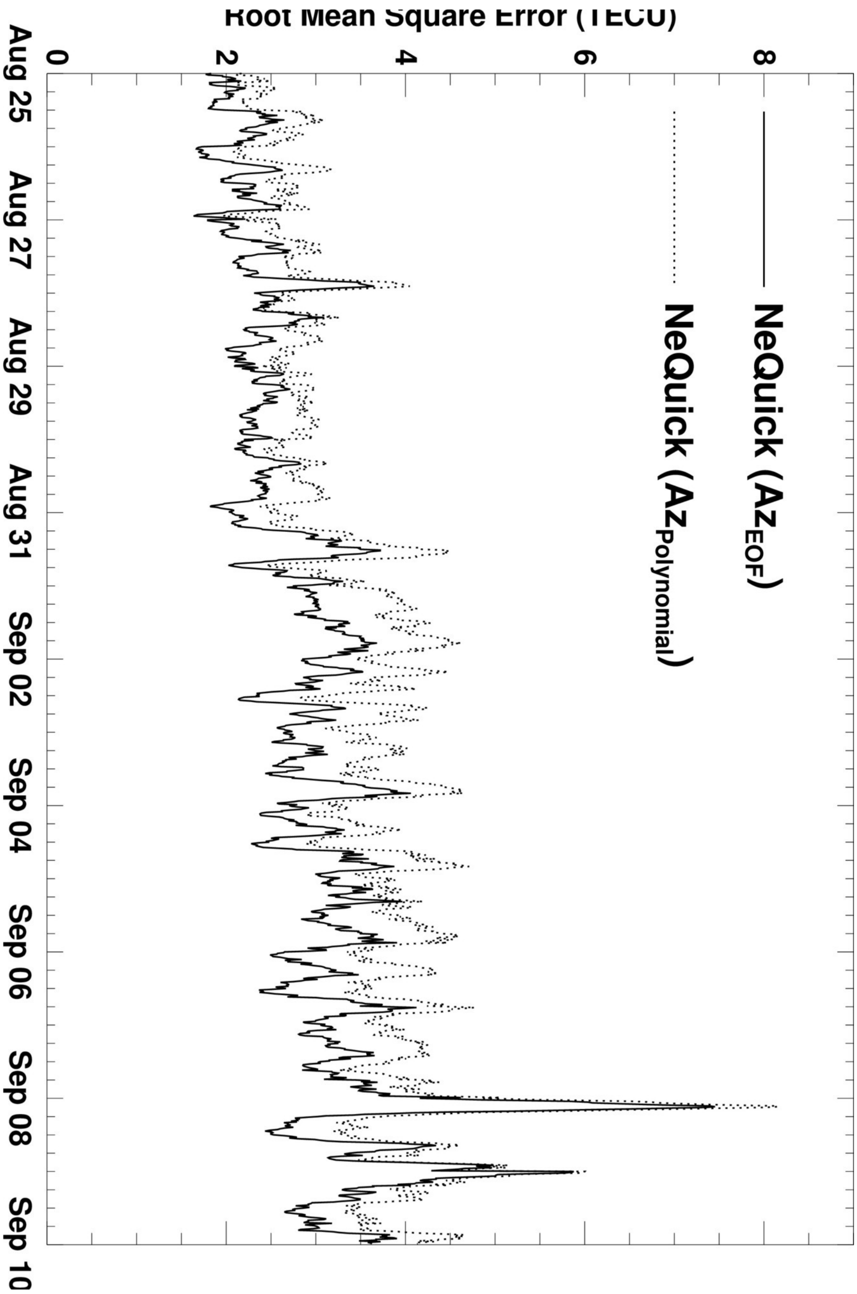

2018sw001987-f09-z-.eps